Computational Study of Reaction Pathways for the Formation of Indium Nitride from Trimethylindium with HN_3: Comparison of the Reaction with NH_3 and That on TiO_2 Rutile (110) Surface†

Yi-Ren Tzeng,*,‡ P. Raghunath,*,‡ Szu-Chen Chen,‡ and M. C. Lin‡,§

Center for Interdisciplinary Molecular Science, Institute of Molecular Science, National Chiao Tung University, Hsinchu 300, Taiwan, and Department of Chemistry, Emory University, Atlanta, Georgia 30322

Received: December 29, 2006; In Final Form: February 10, 2007

The reactions of trimethylindium (TMIn) with HN_3 and NH_3 are relevant to the chemical vapor deposition of indium nitride thin film. The mechanisms and energetics of these reactions in the gas phase have been investigated by density functional theory and ab initio calculations using the CCSD(T)/Lanl2dz//B3LYP/Lanl2dz and CCSD(T)/Lanl2dz//MP2/Lanl2dz methods. The results of both methods are in good agreement for the optimized geometries and relative energies. These results suggest that the reaction with HN_3 forms a new stable product, dimethylindiumnitride, $CH_3-In{=}N-CH_3$ via another stable $In(CH_3)_2N_3$ (dimethylindium azide, DMInA) intermediate. DMInA may undergo unimolecular decomposition to form CH_3InNCH_3 by two main possible pathways: (1) a stepwise decomposition process through N_2 elimination followed by CH_3 migration from In to the remaining N atom and (2) a concerted process involving the concurrent CH_3 migration and N_2 elimination directly giving $N_2 + CH_3InNCH_3$. The reaction of TMIn with NH_3 forms a most stable product $DMInNH_2$ following the initial association and CH_4-elimination reaction. The required energy barrier for the elimination of the second CH_4 molecule from $DMInNH_2$ is 74.2 kcal/mol. Using these reactions, we predict the heats of formation at 0 K for all the products and finally for InN which is 123 ± 1 kcal/mol predicted by the two methods. The gas-phase reaction of HN_3 with TMIn is compared with that occurring on rutile TiO_2 (110). The most noticeable difference is the high endothermicity of the gas-phase reaction for InN production (53 kcal/mol) and the contrasting large exothermicity (195 kcal/mol) released by the low-barrier Langmuir−Hinshelwood type processes following the adsorption of TMIn and HN_3 on the surface producing a horizontally adsorbed InN(a), Ti−NIn−O(a), and other products, $CH_4(g) + N_2(g) + 2CH_3O(a)$ [*J. Phys. Chem. B* **2006**, *110*, 2263].

Introduction

Indium nitride is an important III-nitride semiconductor with a stable wurtzite crystal structure; it has been used for visible optoelectronics, high-efficiency solar cell, and other potential applications.[1−4] This chemically stable and robust InN has a useful range of band gaps, 0.7−2.1 eV, which result from the crystallinity and quantum confinement effects.[5−9] Deposition of InN films of varying thickness on TiO_2 nanoparticle films has been demonstrated by low-pressure organometallic chemical vapor deposition (OMCVD) near 700 K with continuous UV irradiation using hydrazoic acid (HN_3) and trimethylindium (TMIn), which are perhaps the most efficient precursors.[6,9,10] The resulting InN films on TiO_2 exhibit a broad UV/visible absorption between 390 and 800 nm quite similar to that of Graetzel's "black" dye,[11] indicating a promising possibility for photovoltaic applications.[10c]

The main aim of this work is to study the various reaction pathways of acid (HN_3) and base (NH_3) with trimethylindium that may be involved in the chemical vapor deposition of InN using the density functional theory (DFT) and ab initio calculations. Recent work on indium metal complexes has shown that the widely used B3LYP and MP2 methods with Lanl2dz basis sets are quite suitable for geometry and property predictions.[12] Especially, we hope to examine the mechanistic difference between the interaction of TMIn with acid and base in terms of initial reactant complexation and to ensure fragmentation of the association complexes. These studies explore the stability and structural properties of the various possible species, which we believe could help in predictions of the formation of InN in the gas phase and on semiconductor surfaces. The calculated geometries and heats of formation could be helpful for the likely identification of the species in the laboratory.

Computational Methods

The equilibrium geometries of the reactants, transition states, intermediates, and products for the HN_3 and NH_3 with TMIn reactions are optimized by DFT at the B3LYP level and ab initio at the MP2 level using the Gaussian 03 program.[13] The B3LYP method consists of Becke's three-parameter hybrid exchange function combined with the Lee−Yang−Parr correlation function.[14] Due to the limitation of available basis set for the indium atom, our calculations are limited to the approximation of effective core potentials, among which we selected the Los Alamos effective core potential plus double-ζ (lanl2dz) as the basis set.[16] All the geometries are analyzed by harmonic vibrational frequencies obtained at the same level and characterized as minima (no imaginary frequency) or as a transition state (one imaginary frequency). Transition-state geometries are then used as an input for intrinsic reaction coordinate (IRC) calcula-

† Part of the special issue "M. C. Lin Festschrift".

* Corresponding authors. E-mail: yiren.tzeng@gmail.com (Y.-R.T); raghuputikam@yahoo.com (P.R.).

‡ National Chiao Tung University.

§ Emory University.

10.1021/jp0690345 CCC: $37.00
Published on Web 03/28/2007

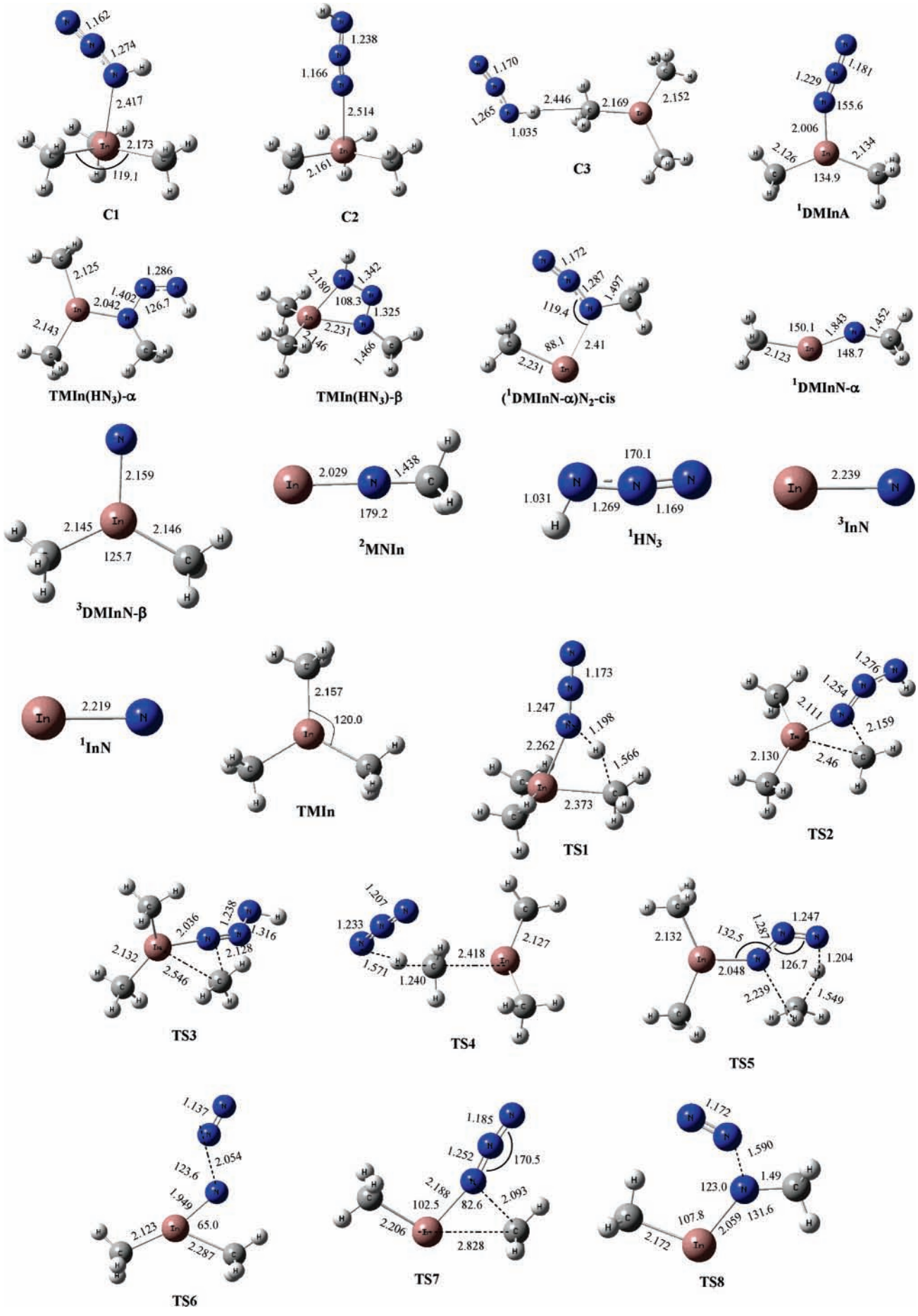

Figure 1. Part 1 of 2.

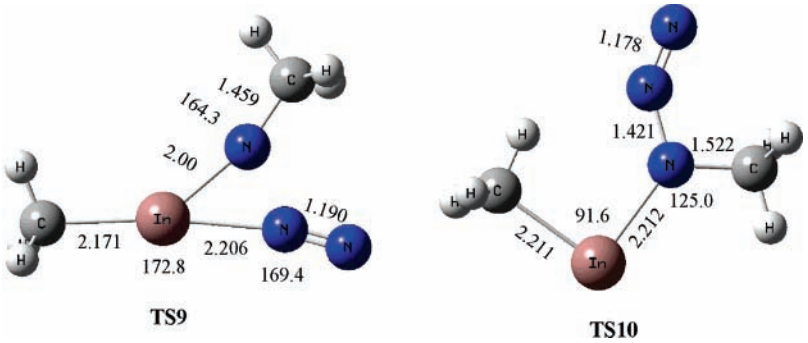

Figure 1. Part 2 of 2. All optimized geometries of the intermediates and the transition states calculated using the B3LYP/Lanl2dz level. Bond lengths are in angstroms and angles in degrees.

TABLE 1: Relative Energies (kcal/mol) of Various Species in the TMIn + HN_3 Reaction Calculated at the Different Levels

species	B3LYP/Lanl2dz + ZPVE	MP2/Lanl2dz + ZPVE	CCSD(T) Lanl2dz//B3LYP/Lanl2dz + ZPVE	CCSD(T) Lanl2dz//MP2/Lanl2dz + ZPVE
$^1HN_3$+ ^{1}TMIn	0.0	0.0	0.0	0.0
NNN(H)−In$(CH_3)_3$, C1	−9.8	−12.5	−13.1	−13.3
HNNN−In$(CH_3)_3$, C2	−5.1	−7.2	−6.8	−6.9
NNN(H)−(CH_3)In$(CH_3)_2$, C3	−1.7	−2.1	−1.7	−1.8
TS1	2.6	2.2	8.2	8.7
TS2	23.0	39.3	26.3	25.4
TS3	31.0	49.6	34.6	33.1
TS4	35.8	32.1	43.8	42.3
^{1}TMIn(HN_3)-α	−21.5	−10.1	−21.0	−21.4
^{1}TMIn(HN_3)-β	−45.7	−32.3	−43.7	−43.9
TS5	28.7	34.1	31.1	28.8
^{1}DMInA + $[CH_4]$	−35.7	−45.2	−34.6	−33.7
TS6 + $[CH_4]$	32.4	26.2	14.9	15.9
TS7 + $[CH_4]$	39.7	41.8	37.8	39.3
^{1}DMInN−α-N_2(cis) + $[CH_4]$	−0.5	−1.3	−4.4	−4.6
^{1}DMInN-α-N_2(trans) + $[CH_4]$	7.6	5.3	2.7	6.2
TS8 + $[CH_4]$	4.9	1.5	−4.7	−3.1
TS9 + $[CH_4]$	8.7	14.5	6.1	2.6
TS10 + $[CH_4]$	18.8		16.8	
^{1}DMInN-α + $[CH_4 + N_2]$	−21.0	−43.4	−41.1	−40.2
^{3}DMInN-α + $[CH_4 + N_2]$	−8.8	−18.6	−23.9	−22.2
^{3}DMInN-β + $[CH_4 + N_2]$	4.0	−13.2	−17.0	−16.2
^{1}DMInN-β + $[CH_4 + N_2]$	41.3	30.1	20.5	21.1
^{2}MNIn + $[CH_4 + N_2 + CH_3]$	9.3	−5.5	−13.6	−12.4
^{3}InN + $[CH_4 + N_2 + 2(CH_3)]$	88.6	63.9	53.3	54.7
^{1}InN + $[CH_4 + N_2 + 2(CH_3)]$	131.7	110.4	94.0	95.3

tions to confirm the transition state is connected to the designated reactants and products.[16] The higher-order correlation energy corrections of both B3LYP and MP2 energies were obtained at a single point using the CCSD(T)/LANL2DZ method.[17] We find the two popular optimization methods give rise to very similar geometries and relative energies, which are also very close to the single point calculation results by CCSD(T) with the geometries predicted with both methods. Zero-point vibrational energy (ZPVE) corrections based on the unscaled frequencies are applied to all of the calculated energies.

As alluded to above, one of the major purposes of this study is to compare the difference between the HN_3 + TMIn reaction pathways in the gas phase and those on the TiO_2 rutile (110) surfaces.[18] Reference 18 used the Vienna ab initio simulation package (VASP) for geometrical optimization with a plane wave basis set. The exchange-correlation function was treated with the local-density approximation (LDA). The generalized gradient approximation (GGA) used for the total energy calculations was that of the Perdew−Wang 1991 (PW91) formulation, which has been shown to work well for surfaces.

Results and Discussion

TMIn + HN_3 Reaction. As aforementioned, the geometries of all the gas-phase reactants, intermediates, products, and transition states have been optimized at the B3LYP/Lanl2dz and MP2/Lanl2dz levels of theory; the results are similar. Therefore we show only the B3LYP results given in Figure 1. The predicted energies with both basis sets, summarized in Table 1, are also very close, particularly after additional single-point calculations with the CCSD(T)/Lanl2dz level. The potential energy diagram obtained at the CCSD(T)/Lanl2dz//B3LYP/Lanl2dz level of theory is presented in Figure 2. The relative energies are calculated with respect to the reactants In$(CH_3)_3$ + HN_3. Because there exist several molecular intermediates, whose triplet-state energies are closer to or lower than those of the corresponding singlet states, to distinguish them, we connect the adiabatic (singlet-to-singlet) reaction pathways with (regular) dashed lines and the nonadiabatic (singlet-to-triplet) surface crossing ones with long and thick dashed lines. The following discussions will be based on the results of the calculations at the CCSD(T)/Lanl2dz//B3LYP/Lanl2dz level of theory.

To facilitate the discussion that follows, we will designate the HN_3 atoms in the N(1)N(2)N(3)H(4) order. Trimethylindium is a planar molecule, and the bond length of In−C is 2.157 Å with low-energy rotational barriers for the methyl groups. In a short range, as shown in region I in Figure 2, we found HN_3 reacting with TMIn can form three molecular complexes, which

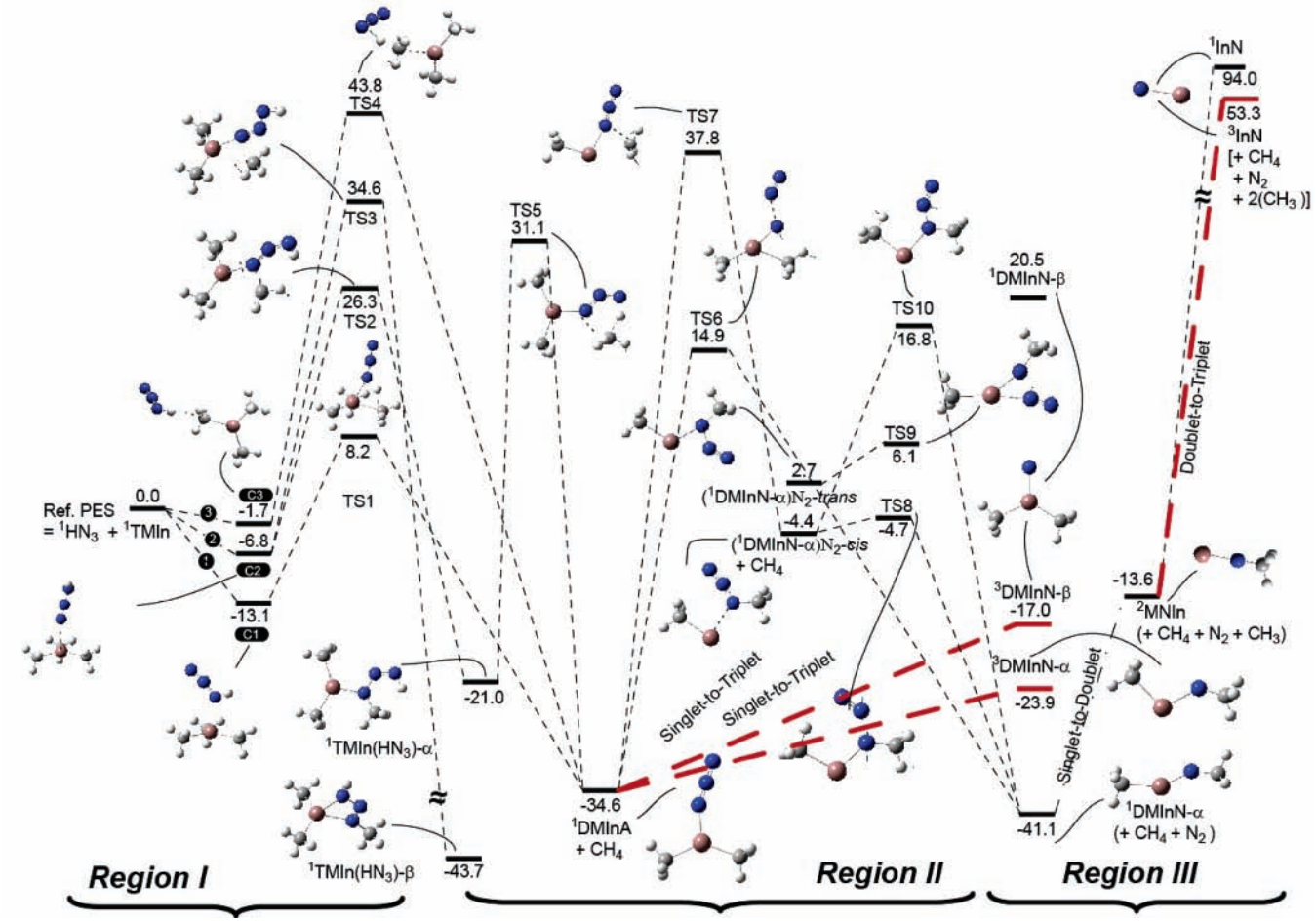

Figure 2. Potential energy surface of the HN_3 + TMIn reaction. Relative energies (kcal/mol) calculated using the CCSD(T)/Lanl2dz//B3LYP/Lanl2dz method.

are denoted as NNN(H)−$In(CH_3)_3$ (C1), HNNN−$In(CH_3)_3$ (C2), and NNN(H)-$(CH_3)In(CH_3)_2$ (C3). In the initial steps, the most reactive N(3) atom bonding with H in HN_3 can directly associate with the indium atom in $In(CH_3)_3$ by a barrierless process that forms with NNN(H)−$In(CH_3)_3$ and exothermic complexation processes. The exothermicities are around 13.1 kcal/mol at the CCSD(T)/Lanl2dz//B3LYP/Lanl2dz level. As shown in Figure 1, nitrogen points toward the In atom in the top and middle of the molecule at a distance of 2.417 Å (2.441 Å by MP2). The complex has C_1 symmetry, and the C−In−C angle has changed from 120 to 119.1°. The second possible initial reaction, N(1) of HN_3 addition toward the In atom of TMIn, to form a complex, C2, has a 6.8 kcal/mol binding energy. Here the bond length of In−N is 2.514 Å. The formation of complex C3 corresponds to the head on approach of H(4) of HN_3 toward one of the CH_3 groups of TMIn and has 1.7 kcal/mol binding energy calculated at the CCSD(T)//B3LYP method. The geometry of the $In(CH_3)_3$ fragment in the complex shows very little change in one of the In−C bond length 2.169 Å (compared to an isolated $In(CH_3)_3$).

In the next reaction step, the two molecular complexes C1 and C3 lie below the reactants by 13.1 and 1.7 kcal/mol and the H(4) atom of the HN_3 can react with one of the methyl groups intramolecularly to eliminate CH_4, producing DMInA (dimethylindium azide), $(CH_3)_2InN_3$, via TS1 and TS4, respectively. This CH_4 elimination process is predicted to have a low potential barrier (TS1) of 21.3 kcal/mol with a large exothermicity that lies −21.5 kcal/mol below that of the reactant C1. The transition vector is dominated by the motion of hydrogen, which is 1.198 Å from the nitrogen and 1.566 Å from the carbon. The large exothermicity mainly shows in part from the formation of the strong C−H bond in part from the weak C−In bond. Relatively, the CH_4 elimination process in C3 needs to go over a much higher potential barrier via the TS4 transition state, the C3 first stretches the N(3)−H and In−CH_3 bonds, and then using the N(3) as a pivotal point, the whole N_3, leading by the N(1), swings toward the In atom with the In−N bond length of 4.350 Å. As N(1) approaches the In atom, the CH_4 detaches from the In to form DMInA. This process has a potential barrier of 45.5 kcal/mol and an exothermicity of −32.9 kcal/mol.

On the basis of the schematic potential energy surface (PES) presented in Figure 2, comparing with C1 and C3 the C2 exhibits a much more complex decomposition and isomerization process. Because the N_3 in HN_3 is approximately linear and sits nearly perpendicularly on the plane of TMIn in C2, the distance between the H(4) and any CH_3 group is too long (>5.70 Å) to allow for a direct CH_4 elimination. As a result of this geometry limitation, the C2 preferably undergoes isomerization processes, leading to the formation of two stable molecules. One of the processes, going through TS2 with a barrier of 33.1 kcal/mol, involves the migration of one CH_3 group toward N(1). This brings the CH_3 group closer to the H(4), allowing the linear N_3 in HN_3 to bend in the direction bringing the CH_3 group even closer to the H(4). This rearrangement leads to the formation of a stable planar C_s symmetry TMIn(HN_3)-α molecule, whose H(4)−CH_3 distance now becomes 2.359 Å and whose energy lies −14.2 kcal/mol below the C2 complex.

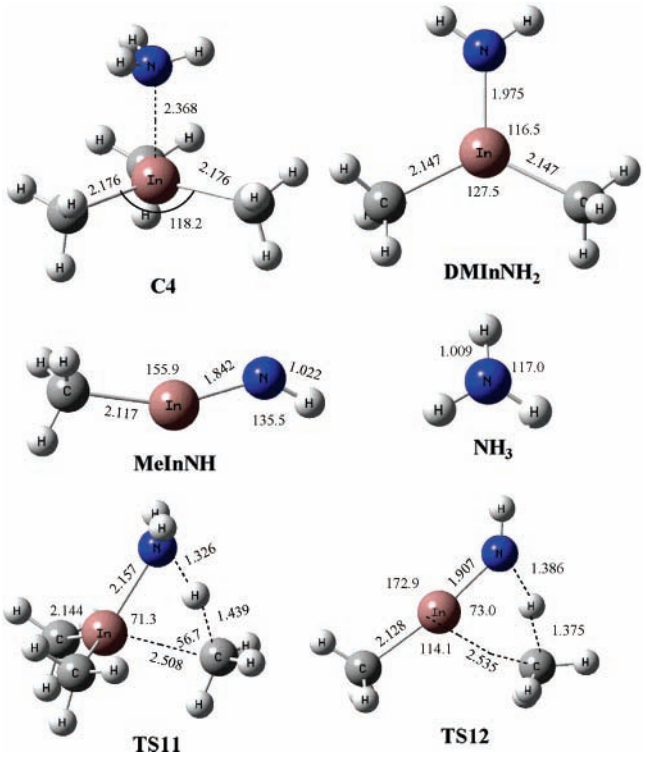

Figure 3. All optimized geometries of the intermediates and the transition states calculated using the B3LYP/Lanl2dz level. Bond lengths are in angstroms and angles in degrees.

The migration of the CH_3 group in C2, as mentioned above, can go through a slightly higher barrier 41.4 kcal/mol TS3 transition state. This causes the N_3 to bend in the opposite direction, which increases the distance between the H(4) atom and the attacked CH_3 group, and brings the N(3) toward the In atom. This process leads to the formation of a stable ringlike TMIn(HN_3)-β molecule. This molecule has a C_s symmetry with planar structure formed by the H, three N, and the attacked C and In atoms, and the distance between the H(4) and three C atoms in each CH_3 group is roughly the same (4.363, 4.363, and 4.323 Å). Because of the large H(4)−CH_3 group distance in the TMIn(HN_3)-β, we did not carry out further search for any possible CH_4 elimination pathway. The energy level of TMIn(HN_3)-β lies −36.9 kcal/mol below the C2 complex.

Further decomposition of TMIn(HN_3)-α produces the DMInA and CH_4 through a CH_4 elimination process, by which the H(4) migrates toward the CH_3 group connected to the N(1) atom. The H(4) appears to bond strongly to the N(3) atom, as we observe that the migration of the H(4) is accompanied by a bending of the N(1)−N(2)−N(3) angle of 126.7°. Also because this process needs to break a strong N−CH_3 bond, the CH_4 elimination process goes through the TS5 transition state with a barrier of 52.1 kcal/mol, even though the exothermicity is −13.6 kcal/mol.

As seen from the PES in region II in Figure 2, the decomposition of DMInA produces the most stable CH_3InNCH_3 denoted as DMInN-α and N_2 molecule. This process may proceed via two branched pathways, both of which are going through high potential barriers. This concerted process involving the concurrent CH_3 migration and N_2 elimination requires the 49.5 kcal/mol energy barrier at TS6. Another channel is a two-step process. The first step, going through the TS7 transition state with a potential barrier of 72.4 kcal/mol, is an isomerization process, involving the migration of one CH_3 from the In atom to the closest N atom to form the (DMInN-α)N_2-cis structure. The second step is a unimolecular decomposition process, which can either go through TS8 (NNNIn-cis) with a barrier of 0.3 kcal/mol or TS10 (NNNIn-trans) with a barrier of 21.2 kcal/mol predicted by the CCSD(T)//B3LYP method. Thus, starting from DMInA, its isomerization by methyl migration to (DMInN-α)N_2-cis is endothermic by 30.2 kcal/mol. The following fast fragmentation of the latter isomer via TS8 is exothermic by 36.7 kcal/mol. It is interesting to note that the (DMInN-α)-N_2-cis may also undergo a cis-to-trans isomerization process, with the trans lying 7.1 kcal/mol higher than the cis. The trans isomer has a low-energy barrier (3.4 kcal/mol) for N_2 elimination via TS9. We also calculated the energy of the optimized singlet DMInN-β, which is an isomer of the singlet DMInN-α. Perhaps because of the ring strain and the open shell N electronic structure, the singlet DMInN-β lies + 61.6 kcal/mol above the singlet DMInN-α.

Up to now, we have assumed that the reaction proceeds adiabatically and thus restricted our calculations to the singlet electronic state. Notwithstanding, because the optimized singlet DMInN-β geometry is rather unstable and much higher in energy than the singlet DMInN-α, the bonding order of the N(3) atom therein gives rise to open-shell electronic structure. We suggest that the N_2 elimination process could give rise to a triplet N(3) forming the triplet DMInN-β shown in Figure 1 and singlet N_2. As seen from the PES in region III in Figure 2, the calculations predict the triplet DMInN-β to be stable and its energy is 37.5 kcal/mol lower than the singlet DMInN-β. Comparatively, the energy level of the triplet DMInN-α is 17.2 kcal/mol higher than the singlet (DMInN-α).

A stepwise unimolecular decomposition of the DMInN-α produces doublet radicals of MNIn and CH_3. In this process, breaking of CH_3 from indium requires 30.3 kcal/mol predicted at B3LYP/Lanl2dz and 27.5 kcal/mol energy at the CCSD(T)//B3LYP level. Similarly, the endothermicity for the reaction of MNIn → InN + CH_3, which breaks the CH_3 from the N atom, is 66.9 kcal/mol and triplet InN lies 40.7 kcal/mol below the singlet InN.

Comparison with the TMIn + NH_3 Reaction. It is interesting to compare the TMIn + HN_3 reaction with the TMIn + NH_3 reaction. The calculated structures of intermediates, transition states, and products of all investigated steps are given in Figure 3, and relative energies are given in Table 2.

TABLE 2: Relative Energies (kcal/mol) of Various Species in the TMIn + NH_3 Reaction Calculated at the Different Levels

species	B3LYP/Lanl2dz + ZPVE	MP2/Lanl2dz + ZPVE	CCSD(T) Lanl2dz//B3LYP/Lanl2dz + ZPVE	CCSD(T) Lanl2dz//MP2/Lanl2dz + ZPVE
NH_3 + TMIn	0.0	0.0	0.0	0.0
$(CH_3)_3In-NH_3$, C4	−17.4	−19.6	−20.0	−19.8
TS11	9.2	12.8	14.3	14.2
$DMInNH_2 + CH_4$	−22.2	−22.5	−22.6	−22.5
TS12 + CH_4	47.5	50.1	51.6	51.4
MeInNH + $2CH_4$	25.5	19.6	19.7	19.9
^{2}InNH + CH_3 + $2CH_4$	64.1	62.2	52.7	53.6
^{3}InN + H + CH_3 + $2CH_4$	160.7	146.0	136.0	136.8
^{1}InN + H + CH_3 + $2CH_4$	203.9	192.5	176.8	177.4

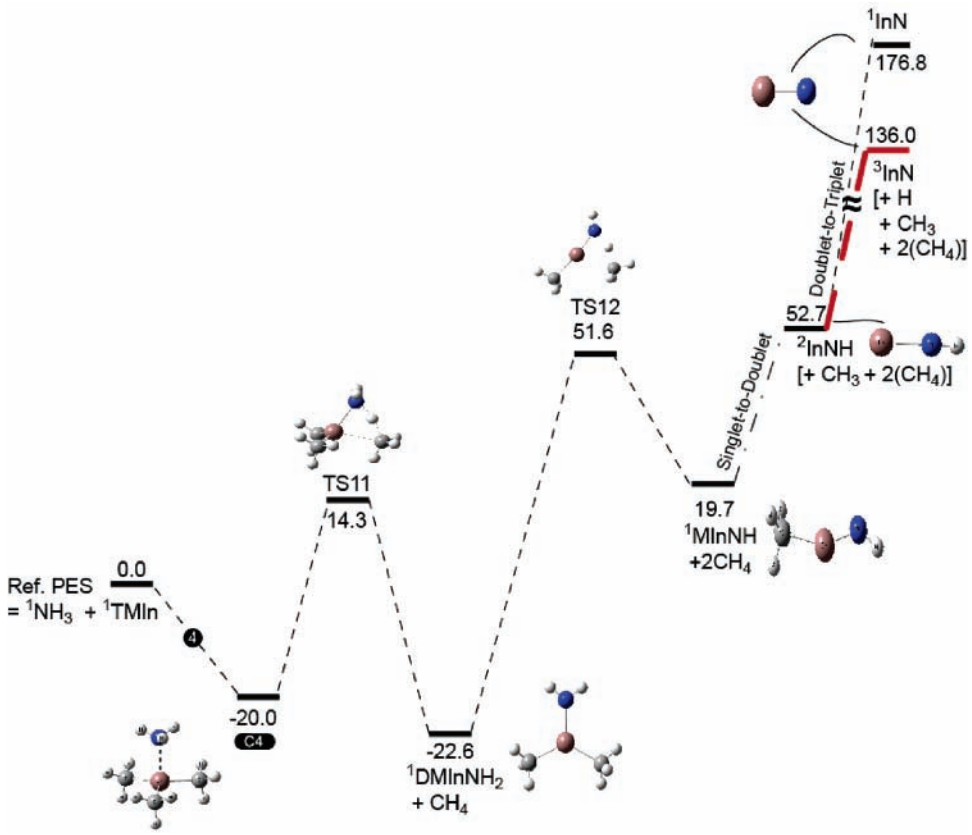

Figure 4. Potential energy surface of the NH_3 + TMIn reaction. Relative energies (kcal/mol) are calculated using the CCSD(T)/Lanl2dz//B3LYP/Lanl2dz method.

The potential energy diagram obtained at the CCSD(T)/Lanl2dz//B3LYP/Lanl2dz level of theory is presented in Figure 4. The association reaction of the electron deficient TMIn and NH_3 can form the C4 molecular complex with a calculated binding energy of 20.0 kcal/mol, which is more stable than C1, the most stable $(CH_3)_3In-N(H)N_2$ complex. This 20 kcal/mol binding energy of C4 may be compared with previous calculations of binding energy of 18.2 kcal/mol for $(CH_3)_3In-NH_3$ using the B3LYP/Lanl2dz* level.[12e] The structure of the $(CH_3)_3In-NH_3$ complex has been previously discussed in detail, and the calculated In−N bond length of 2.368 Å agrees well with previous calculations.[12e] The decomposition of the $(CH_3)_3In-NH_3$ molecular complex to the most stable intermediate $DMInNH_2$, $(CH_3)_2InNH_2$, and a CH_4 molecule requires the transition-state energy at TS11 of 34.3 or 14.3 kcal/mol above the reactants predicted at the CCSD(T)//B3LYP level of theory. In this PES, the formation of products $DMInNH_2 + CH_4$ is most exothermic with 22.6 kcal/mol exothermicity. This amount of energy release is somewhat smaller than that of the analogous CH_4-elimination reaction of C1, producing DMInA, 34.6 kcal/mol. $DMInNH_2$ can further undergo a CH_4-elimination process, by which the H migrates toward the CH_3 group connected to the In atom to form MInNH at 19.7 kcal/mol above the reactants. The CH_4-elimination process goes through the TS12 transition state with a high-energy barrier of 74.2 kcal/mol. There is no analogous step in the TMIn−HN_3 system, but the fragmentation of DMInA to produce CH_3InNCH_3 (DMInN-α) + N_2 has to overcome only about a 50 kcal/mol barrier. We could not locate a saddle point for the generation of InN and CH_4 from MInNH. The energy required for MInNH to decompose into InNH + CH_3 is 33.0 kcal/mol. It further dissociates without barrier to produce ^{3}InN + H with an overall endothermicity of 83.3 kcal/mol from ^{2}InNH. Singlet InN is 40.8 kcal/mol above the triplet InN + H.

TABLE 3: Heats of Reaction ($\Delta_r H_0°$, kcal/mol) and Heats of Formation ($\Delta_f H_0°$, kcal/mol) of Species at 0 K Predicted at the CCSD(T)/Lanl2dz//B3LYP/Lanl2dz Level of Theory

species	reaction[a]	$\Delta_r H_0°$	$\Delta_f H_0°$
	TMIn + HN_3		
C1	$HN_3 + (CH_3)_3In \rightarrow$ C1	−13.1	111.7
DMInA	C1 → DMInA + CH_4	−21.5	106.2
DMInN	DMInA → DMInN + N_2	−6.5	99.7
MNIn	DMInN → MNIn + CH_3	27.5	91.3
InN	MNIn → InN + CH_3	66.8	122.3
	TMIn + NH_3		
C4	$NH_3 + (CH_3)_3In \rightarrow$ C4	−20.0	23.7
$DMInNH_2$	C1 → $DMInNH_2 + CH_4$	−2.6	37.1
MInNH	$DMInNH_2 \rightarrow$ MInNH + CH_4	42.3	95.4
InNH	MInNH → InNH + CH_3	32.9	92.5
InN	InNH → InN + H	83.3	124.2

[a] The experimental values are obtained on the basis of the following heats of formation at 0 K: $(CH_3)_3In$, 52.97 kcal/mol (calculated from the 298 K value given in ref 19 using vibrational frequencies in this work); HN_3, 71.8 kcal/mol;[22] NH_3, −9.30 kcal/mol;[20] CH_4, −16.0 ± 0.08 kcal/mol;[20] CH_3, 35.86 ± 0.07 kcal/mol;[21] H, 51.65 kcal/mol.[20]

Heats of Formation. The predicted heats of formation of InN presented in Table 3 were based on the energies computed at the CCSD(T)/Lanl2dz//B3LYP/Lanl2dz level using TMIn reacting with HN_3 and NH_3. Based on predicted heats of reactions ($\Delta_r H_0°$) and experimental heats of formation ($\Delta_f H_0°$) of reactants at 0 K, the heats of formation of all intermediate products from both reactions are calculated. Experimentally, the heats of formation are available for the following: $(CH_3)_3In$, 49.9 kcal/mol at 298 K (or 53.0 kcal/mol at 0 K); HN_3, 71.8 kcal/mol; NH_3, −9.3 kcal/mol; and CH_4, −16.0 ± 0.08 kcal/

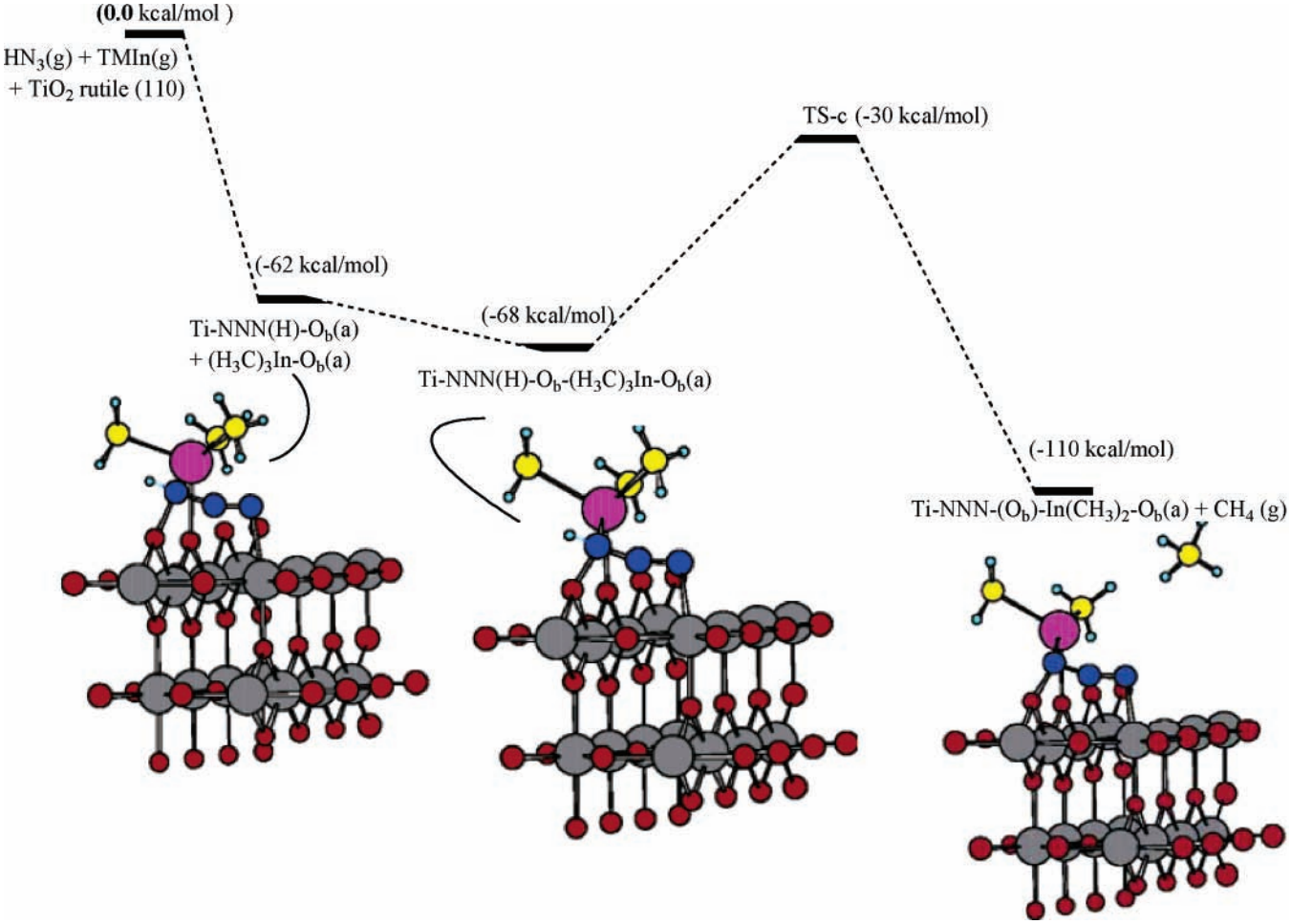

Figure 5. PES of the surface reaction pathways of HN_3 with TMIn on the TiO_2 rutile (110) surfaces. (Redrawn with permission from Figure 2 in ref 18a. Copyright 2006 American Chemical Society.)

mol.[19−22] The predicted $\Delta_f H_0°$ (0 K) for the five products, C1 [NNN(H)−In$(CH_3)_3$], DMInA [$(CH_3)_2InN_3$], DMInN [$(CH_3)_2InN$], MNIn [CH_3InN], and InN, are 111.7, 106.2, 99.7, 91.3, and 122.3 kcal/mol, respectively, and have been estimated, as shown in Table 3. In addition, $\Delta_f H_0°$ (0 K) for these products $(CH_3)_3InNH_3$, $(CH_3)_2InNH_2$, CH_3InNH, InNH, and InN are 23.7, 37.1, 95.4, 92.5, and 124.2 kcal/mol, respectively, which are calculated using the TMIn + NH_3 reaction. The corresponding experimental values are not available. The InN heat of formation determined using the reactions of HN_3 and NH_3 with TMIn is approximately same energy, 122.3 and 124.2 kcal/mol, respectively, at 0 K. Earlier we employed the same method to evaluate the heats of formation of InO and InS; the predicted values were found to be in good agreement with experimental data.[23]

Comparison with Reactions on TiO_2 Rutile (110). Recently, our group has studied the reactions of HN_3 and TMIn on the TiO_2 rutile (110) surface by first-principles calculations based on the DFT and pseudopotential method.[18] Here, we compare the reaction mechanism of the lowest energy pathways of the gas-phase and TiO_2 surface reactions and how the TiO_2 rutile (110) surfaces affect the HN_3 + TMIn reactions. For comparison purposes, we have rearranged the reference potential[18a] in Figure 5 to the energy of the most stable adsorbates, which corresponds to the HN_3(g) + TMIn(g) + TiO_2 rutile (110) [see Figure 2 in ref 18a].

Both the reaction pathways in the gas phase and on the TiO_2 surface are very similar. On the clean rutile (110) surface, TMIn and HN_3 can molecularly coadsorb on the surface, giving $(H_3C)_3In-O_b(a)$ and Ti−NNN(H)−O_b(a) with a total of 62 kcal/mol adsorption energy, where O_b denotes a bridged O atom.[18a] The reaction proceeds initially with the approach of the N(3) atom of HN_3 toward the In atom to form a most stable Ti−NNN(H)−O_b−$(H_3C)_3In-O_b$(a) molecular complex. The exothermicity of the above the association complex is 68 kcal/mol. A similar CH_4-elimination process yielding CH_4(g) and Ti−NNN−(O_b)−$In(CH_3)_2-O_b$(a) takes place with a 38 kcal/mol barrier which lies 30 kcal/mol below the reactants, HN_3(g) + TMIn(g) + TiO_2 rutile (110); the reaction is exothermic by 42 kcal/mol (or 110 kcal/mol exothermic from the reactants). The overall reaction exothermicity producing Ti−InN−O(a) + CH_4(g) + $2CH_3O$(a) + N_2(g) was predicted to be 195 kcal/mol, where Ti−InN−O(a) is an InN molecule adsorbed horizontally on the TiO_2 surface.[18a] The gas−surface reaction of TMIn + HN_3 is therefore very exothermic and can occur easily on TiO_2 surfaces, as has been demonstrated experimentally by Wang and Lin.[10,18]

Conclusions

In this work, we have presented the reaction mechanisms for the reactions of TMIn with HN_3 and NH_3, investigated by DFT (B3LYP) and ab initio (MP2) methods. We predicted that the lowest energy pathway for the HN_3 and NH_3 + TMIn reactions proceeds by first forming molecular complexes NNN(H)−$In(CH_3)_3$ (C1) and $(CH_3)_3In-NH_3$ (C4) followed by a CH_4-elimination process which goes over a potential barrier of 21.3 and 34.3 kcal/mol to form the $DMInN_3$ and $DMInNH_2$, respectively. Then $DMInN_3$ undergoes a concerted process

involving the concurrent CH_3 migration and N_2 elimination which requires 49.5 kcal/mol energy barrier to form DMInN (CH_3InNCH_3). Subsequently, by two series of stepwise CH_3 decomposition, DMInN breaks into InN and two CH_3 radicals. The energy of the triplet InN is 40.7 kcal/mol lower than the singlet. In the case of NH_3 reaction the elimination of two CH_4 molecules to form MInNH requires a high-energy barrier of 74.2 kcal/mol. The MInNH thus formed can decompose into InNH and CH_3 and finally into InN and H radicals. The total energy required for this process is 83.3 kcal/mol. From these two reactions we calculated the heat of formation of InN at 0 K to be 122.3 and 124.2 kcal/mol. Contrary to the gas-phase processes which produce InN endothermically as alluded to above, the reaction of TMIn with HN_3 on the rutile TiO_2 (110) surface via the Langmuir−Hinshelwood mechanism was found to be very exothermic with the final production of an InN molecule horizontally adsorbed on the rutile surface.[18a]

Acknowledgment. The authors thank the Institute of Nuclear Energy Research (INER), Taiwan, for the funding of this project. M.C.L. acknowledges the support from the Taiwan Semiconductor Manufacturing Co. for TSMC Distinguished Professorship and for the National Science Council of Taiwan for the Distinguished Visiting Professorship at National Chiao Tung University in Hsichu, Taiwan.

References and Notes

(1) Juza, R.; Hahn, H. *Z. Anorg. Allg. Chem.* **1938**, *239*, 282.

(2) Jain, M.; Willander, M.; Narayan, J.; Overstraten, R. V. *J. Appl. Phys*. **2000**, *87*, 965.

(3) Strite, S.; Morkoc, H. *J. Vac. Sci. Technol., B.* **1992**, *10*, 1237.

(4) Bhuiyan, A. G.; Hashimoto, A.; Yamamoto, A. *J. Appl. Phys.* **2003**, *94*, 2779.

(5) Xu, K.; Yoshikawa, A. *Appl. Phys. Lett.* **2003**, *83*, 251.

(6) Wakahara, A.; Tsuchiya, T.; Yoshida, A. *J. Cryst. Growth* **1990**, *99*, 385.

(7) Matsuoka, T.; Okamoto, H.; Nakao, M.; Harima, H.; Kurimoto, E. *Appl. Phys. Lett.* **2002**, *81*, 1246.

(8) Yodo, T.; Yona, H.; Ando, H.; Nosei, D.; Harada, Y. *Appl. Phys. Lett.* **2002**, *80*, 968.

(9) Hwang, J.-S.; Wu, C. T.; Chen, K.-H, Chuan, C. M.; Chen, L.-C.; Chen, T. T.; Chen, Y. F.; Lin, M. C. Unpublished work.

(10) (a) Bu, Y.; Ma, L.; Lin, M. C. *J. Vac. Sci. Technol., A* **1993**, *11*, 2931. (b) Bu, Y.; Ma, L.; Lin, M. C. *Mater. Res. Soc. Symp. Proc.* **1993**, *335*, 21. (c) Wang, J. H.; Lin, M. C. *ChemPhysChem.* **2004**, *5*, 1615.

(11) Nazeeruddin, M.-K.; Kay, A.; Rodicio, I.; Humpry-Baker, R.; Muller, E.; Liska, P.; Vlachopoulos, N.; Graetzel, M. *J. Am. Chem. Soc.* **1993**, *115*, 6328.

(12) (a) Cardelino, B. H.; Moore, C. E.; Cardelino, C. A.; Frazier, C. A.; Bachmann, K. J. *J. Phys. Chem. A* **2001**, *105*, 849. (b) Rothschopf, G. K.; Perkins, J. S.; Li, S.; Yang, D.-S. *Phys. Chem. A* **2000**, *104*, 8178. (c) Himmel, H.-J.; Downs, A. J.; Greene, T. M. *J. Am. Chem. Soc.* **2000**, *122*, 9793. (d) Tachikawa, H.; Kawabata, H. *J. Mater. Chem.* **2003**, *13*, 1293. (e) Nakamura, K.; Makino, O.; Tachibana, A.; Matsumoto, K. *J. Organomet. Chem.* **2000**, *611*, 514.

(13) Frisch, M. J.; Trucks, G. W.; Schlegel, H. B.; Scuseria, G. E.; Robb, M. A.; Cheeseman, J. R.; Montgomery, J. A., Jr.; Vreven, T.; Kudin, K. N.; Burant, J. C.; Millam, J. M.; Iyengar, S. S.; Tomasi, J.; Barone, V.; Mennucci, B.; Cossi, M.; Scalmani, G.; Rega, N.; Petersson, G. A.; Nakatsuji, H.; Hada, M.; Ehara, M.; Toyota, K.; Fukuda, R.; Hasegawa, J.; Ishida, M.; Nakajima, T.; Honda, Y.; Kitao, O.; Nakai, H.; Klene, M.; Li, X.; Knox, J. E.; Hratchian, H. P.; Cross, J. B.; Adamo, C.; Jaramillo, J.; Gomperts, R.; Stratmann, R. E.; Yazyev, O.; Austin, A. J.; Cammi, R.; Pomelli, C.; Ochterski, J. W.; Ayala, P. Y.; Morokuma, K.; Voth, G. A.; Salvador, P.; Dannenberg, J. J.; Zakrzewski, V. G.; Dapprich, S.; Daniels, A. D.; Strain, M. C.; Farkas, O.; Malick, D. K.; Rabuck, A. D.; Raghavachari, K.; Foresman, J. B.; Ortiz, J. V.; Cui, Q.; Baboul, A. G.; Clifford, S.; Cioslowski, J.; Stefanov, B. B.; Liu, G.; Liashenko, A.; Piskorz, P.; Komaromi, I.; Martin, R. L.; Fox, D. J.; Keith, T.; Al-Laham, M. A.; Peng, C. Y.; Nanayakkara, A.; Challacombe, M.; Gill, P. M. W.; Johnson, B.; Chen, W.; Wong, M. W.; Gonzalez, C.; Pople, J. A. *Gaussian 03*, Revision C.02; Gaussian: Wallingford, CT, 2004.

(14) (a) Becke, A. D. *Phys. Rev. A* **1998**, *38*, 3098. (b) Lee, C.; Yang, W.; Parr, R. G. *Phys. Rev. B* **1988**, *37*, 785. (c) Becke, A. D. *J. Chem. Phys.* **1993**, *98*, 5648.

(15) (a) Dunning, T. H., Jr.; Hay, P. J. In *Modern Theoretical Chemistry*; Schaefer, H. F., III, Ed.; Plenum Press: New York, 1977. (b) Hay, P. J.; Wadt, W. R. *J. Chem. Phys.* **1985**, *82*, 270. (c) Wadt, W. R.; Hay, P. J. *J. Chem. Phys.* **1985**, *82*, 284. (d) Hay, P. J.; Wadt, W. R. *J. Chem. Phys.* **1985**, *82*, 299.

(16) (a) Gonzalez, C.; Schlegel, H. B. *J. Chem. Phys.* **1989**, *90*, 2154. (b) Gonzalez, C.; Schlegel, H. B. *J. Phys. Chem.* **1990**, *94*, 5523.

(17) (a) Cizek, J. *Adv. Chem. Phys.* **1969**, *14*, 35. (b) Purvis, g. D.; Bartlett, R. J. *J. Chem. Phys.* **1982**, *76*, 1910. (c) Scuseria, G. E.; Janssen, C. L.; Schaefer, H. F., III. *J. Chem. Phys.* **1988**, *89*, 7382. (d) Scuseria, G. E.; Schaefer, H. F., III. *J. Chem. Phys.* **1989**, *90*, 3700.

(18) (a) Wang, J. H.; Lin, M. C. *J. Phys. Chem. B* **2006**, *110*, 2263. (b) Wang, J. H.; Lin, M. C. *J. Phys. Chem. B* **2005**, *109*, 20858. (c) Wang, J. H.; Lin, M. C.; Sun, Y. C. *J. Phys. Chem. B* **2005**, *109*, 5133.

(19) *NIST Chemistry WebBook*; NIST Standard Reference Database No. 69; National Institute of Standards and Technology: Gaithersburg, MD, 2005; http://webbook.nist.gov/chemistry/.

(20) Chase, M. W., Jr.; Davies, C. A.; Downey, J. R., Jr.; Frurip, D. J.; McDonald, R. A.; Syverud, A. N. JANAF Thermochemical Tables. *J. Phys. Chem. Ref. Data* **1985**, *14*, Suppl. 1.

(21) Ruscic, B.; Litorja, M.; Asher, R. L. *J. Phys. Chem. A* **1999**, *103*, 8625.

(22) Gurvich, L. V.; Veyts, I. V.; Alcock, C. B. *Thermodynamic Properties of Individual Substances*, 4th ed.; Hemisphere: New York, 1989.

(23) Raghunath, P.; Lin, M. C. *J. Phys. Chem*., submitted for publication (revision).